Chapter 3

Fluorescence of Molecules near Aggregated and Isolated Gold Nanoparticles

Fluorescence of Molecules near Aggregated and Isolated Gold Nanoparticles

When a molecular probe is situated close to the metal nanoparticle surface, the fluorescence of the molecules becomes quenched. However, when the nanoparticles are aggregated into assemblies, the fluorescence may be enhanced. Aggregation amongst the colloidal particles could be accomplished by the controlled addition of external reagents or may occur spontaneously (devoid of any chemicals) that is ubiquitous to nanoparticulate systems. Therefore, the emission behavior of the molecular probe is governed by the physical state of nanostructures. In this chapter, we have tried to elucidate the emission behavior of the molecular probes near isolated and aggregated gold nanoparticles. This chapter contains two sub-sections:

3.1 Fluorescence Enhancement in Spontaneous and Induced Aggregated Gold Nanoparticles

3.1.1. Introduction

In recent years, the unique physical and chemical properties of the surfaces of solids have attracted increased attention in scientific parlance.[1] As the size of the particles shrinks into the nanometer regime, there is an increasingly important role of the surface in controlling the overall energy of the particles.[2] Metallic particles at the nanoscale dimension possess high surface-to-volume ratio and therefore, are very prone to rapid and irreversible coalescence. On the other hand, controlled aggregation is of great relevance in colloidal science because of their various technological applications. As a consequence, the aggregation processes in colloids have been the subject of numerous experimental, theoretical and computational studies.[3-5]

Metallic particles, *viz.*, copper, silver and gold, in the nanometer size regime exhibit strong absorption in the visible region, often coined as localized surface plasmon resonances (LSPRs).[6] The physical origin of the light absorption by metal nanoparticles is due to coherent oscillations of the conduction electrons driven by electromagnetic

radiation and are dependent upon the metal and host dielectric functions, particle geometry along with light polarization and wavelength.[7,8] The plasmon resonances of the metal nanoparticles aggregated in a close-packed assembly (especially, when the interparticle distance are less than five times of the particle radius, $d \leq 5R$) are known to be coupled as a result of electrodynamic interaction between the particles.[9] However, the combination of conjugated organic chromophores and metal nanoparticles has emerged to produce a new class of organic-inorganic hybrid assemblies[10-12] which entice scientists and engineers for numerous potential applications, e. g., in optical emitters,[13] nanoscale optical antennas,[14] plasmonic integrated circuits,[15] surface plasmon enhanced light emitting diodes[16] and so on.[17] Metallic nanostructures modify the intrinsic photophysical characteristics of fluorophores in a controllable manner governed by nanoparticle morphology, distance between the molecules and nanoparticles and geometry/orientation of the molecules around the nanoparticle surface.[18] While the molecular probes are allowed to interact with plasmon coupled nanoparticle assemblies, it has been found that the majority of the enhancement takes place at the junction of aggregated particles bringing to light the importance of interparticle interaction.[19] The dependence of the coupled LSPR frequency on the interparticle distance could be used as a ‘‘plasmonic ruler’’ to measure nanometric distances in biological systems.[20] The use of fluorophore-metal interactions in biotechnology has primarily been referred to as metal-enhanced fluorescence or surface-enhanced fluorescence or radiative decay engineering and can be used to develop next-generation biological and chemical sensors.[21]

The study of dipolar coupling of radiative molecules to the surface plasmon of metallic surfaces dates back to the beginning of the 20th century with the theoretical work of Zenneck and Sommerfeld among others.[22, 23] A great deal of theoretical and experimental studies has been performed over the last few decades in understanding the behavior of probe molecules in which the molecular dipole is damped by the nearby metal surface.[18-25] Therefore, it has become quite obvious to study the influence of the variation of particle size, shape, interparticle coupling and local dielectric environment of the nanoparticles for fluorophores deposited nearby metal nanoparticles under carefully optimized conditions. Geddes and co-workers[26] have reported the first observation of metal-enhanced fluorescence by measuring fluorescence emission of fluorescein

isothiocyanate-conjugated human serum albumin on 40 and 200 nm gold colloids deposited onto glass substrates in a homogeneous fashion. It has been found that the fluorescence enhancement is higher with 200 nm gold colloids as compared to 40 nm colloids due to the increased contribution of the scattering portion of the 200 nm gold colloid extinction spectrum. Li and group[27] have shown unusual fluorescence enhancement of a particular carbazolyldiacetylene derivative upon binding onto gold nanoparticles that could be attributed to the effect of restricted intramolecular rotation resulting from nanoparticle aggregation in the organic-inorganic hybrid assemblies. Lv et al.[28] have designed three gold nanoparticle havecomposites protected by perylene bisimide derivatives and it has been seen that the composites render substantial fluorescence enhancement due to the restricted intramolecular rotation/torsion in the packed nanoclusters. The structural effect of the ligands on aggregation-enhanced emission has been studied and temperature-dependent experiments were conducted to demonstrate the mechanism of fluorescence enhancement. Moerner and colleagues[29] observed enhancement of a single molecule's fluorescence up to a factor of 1,340 using gold nanobowties. Electromagnetic simulation reveled that this is a result of greatly enhanced absorption and an increased radiative emission rate, leading to enhancement of intrinsic quantum efficiency. Chen et al.[30] have investigated the correlation of the fluorescence intensity of dyes with the localized surface plasmon resonance of the individual DNA-functionalized silver nanoprisms using dark field scattering and fluorescence microscopy. It has been seen that the dye functionalized silver nanoprisms are highly fluorescent and their fluorescence intensity is a sensitive function of the degree of the spectral overlap between nanoparticle LSPR and the absorption and emission spectra of the dye. Mennucci and group[31] have presented a hybrid quantum mechanical/classical mechanical description to study the role of the solvent and plasmon coupling in the metal enhanced fluorescence in a regular array. The self-consistent field character of the model has allowed to show that the number and the location of the 'hot spots' responsible for fluorescence enhancement are strictly related to the solvent-induced effects of both on the optical properties of the fluorophore and plasmon couplings among the nanoparticles in the array.

In this sub-section, we have employed fluorescein isothiocyanate as local probe in elucidating physicochemical aspects of spontaneously and induced-aggregates of gold nanoparticles of seven different sizes. Gold nanoparticles have been chosen for this experiment as the particles display the most consistent aggregated behavior in the nanostructures. A series of polymer-stabilized spherical gold nanoparticles of variable sizes (< 5 nm) have been synthesized by the borohydride reduction method. Aggregation amongst these ultrasmall gold nanoparticles has been accomplished either by controlled addition of hydrazine or ageing the colloidal dispersion leading to irreversible coalescence. While the FITC molecules were used as molecular probes, the proximity of the dye to gold nanoparticle aggregates results in an increase in intensity of the fluorophores and markedly varies with the size of the gold nanoparticles in the aggregates. Analysis of the salient features reveals that surface plasmon field is different in case of spontaneous and induced-aggregated gold nanoparticles of different sizes. The effect of different concentration of gold nanoparticle aggregates and time of interaction between the dye molecules and nanoparticle aggregates has been studied explicitly.

3.1.2. Experimental

3.1.2.1. Synthesis and Characterization of PVP-Stabilized Gold Nanoparticles of Variable Sizes

Monodisperse gold clusters of variable sizes ranging from 1 to 5 nm have been synthesized by following the method reported by Tsukuda and co-workers.[32] In a typical procedure, an aqueous solution of $HAuCl_4$ was mixed with PVP in different molar ratio (R) and reduced with sodium borohydride for the synthesis of different sets of gold nanoparticles. Firstly, an aqueous solution (20 mL) of requisite amount of PVP (5-100 mM) was stirred for 2 h on an ice-bath maintained at 0 °C. Subsequently, an aliquot of $HAuCl_4.3H_2O$ (0.5 mM) solution was added and the mixture was stirred for 1 h. Then, ice-cold aqueous solution of $NaBH_4$ (0.1 M, 2 mL) was added instantaneously into the mixture under vigorous stirring. The color of the mixture immediately turned from pale yellow to bright brown indicating the formation of small gold nanoparticles. The stirring

Table 3.1. Synthetic Conditions[#] and Characteristic Parameters of the Different Sets of Gold Particles

Set	$[HAuCl_4]$ (mM)	[PVP] (mM)	R= [PVP]/$[HAuCl_4]$	Colour	Avg. diameter (nm)
A	0.5	100.0	200	brown	1.0±0.3
B	0.5	75.0	150	brown	1.5±0.3
C	0.5	50.0	100	brown	2.3±0.4
D	0.5	37.5	75	brown	2.9±0.5
E	0.5	25.0	50	brown	3.5±0.6
F	0.5	12.5	25	brown	4.1±0.6
G	0.5	5.0	10	brown	4.9±0.8

[#]For gold nanoparticle synthesis, the total volume of the solution was 25 mL.

was continued for another half an hr. The particles are stable for a couple of days while stored in the freeze. The variation in synthetic conditions and sizes for different sets of gold particles are summarized in Table 3.1.

3.1.2.2. Synthesis of Gold-Probe Assembly

In a typical set, requisite amount of spontaneous/induced-aggregated gold (1.0 μM) was added to an aqueous solution of FITC (40 nM) and the final volume of the solution was maintained to 3 mL in well-stoppered quartz cuvettes and the fluorescence of each solution was measured in the spectrofluorimeter.

3.1.3. Results and Discussion

3.1.3.1. Photophysical Properties of FITC

Fluorescein isothiocyanate (pK_a ~ 6.7) belongs to hydroxyxanthene dyes and is known for their strong absorption (λ_{abs}~ 494 nm; extinction co-efficient >70,000 M^{-1} cm^{-1}) and emission (λ_{em}~ 519 nm; φ_f ~ 0.95) in the visible region.[33] It is widely used as a fluorescent tracer in many applications, such as, in microscopy, in a type of dye laser as the gain medium, in forensic and serology to detect latent blood stains and as a bio-tagger to elucidate the cellular transport processes.[34] The molecular structure of FITC is shown in Scheme 3.1.

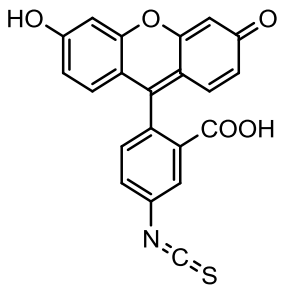

Scheme 3.1. Molecular structure of FITC

3.1.3. 2. Characterization of the Gold Particles

The as-synthesized PVP-stabilized gold particles have been characterized by UV-vis spectroscopy (Figure 3.1**)**. It is seen that the gold particles do not exhibit any prominent surface plasmon band in the visible region rather put a signature at *ca.* 520 nm indicating the formation of ultrasmall gold nanoparticles (< 5 nm). It is now well-established in the literature that the surface plasmon band of gold nanoparticles arises only when the particles are larger than 5 nm.[35] The collective oscillation of the conduction electrons on the metal surface with electromagnetic radiation, so called surface plasmon has not been exhibited, due to extremely small sizes of the gold nanoparticles. Moreover, it is noted that absorbance of the surface plasmon band increases with increasing size of the gold nanoparticles.

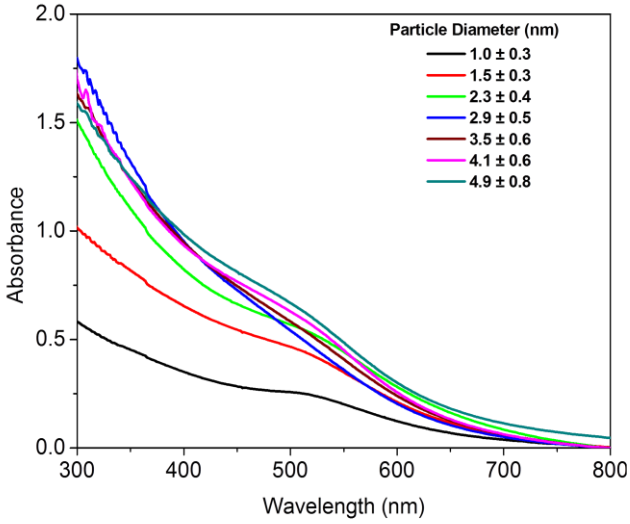

Figure 3.1. UV-vis spectra of the as-synthesized colloidal gold of different sizes.

Transmission electron micrographs of the as-synthesized gold nanoparticles shows that the particles are exclusively spherical with average diameter 1.0 ± 0.3, 1.5 ± 0.3, 2.3 ± 0.4, 2.9 ± 0.5, 3.5 ± 0.6, 4.1 ± 0.6 and 4.9 ± 0.8 nm respectively. Figure 3.2 shows the TEM images of the gold clusters showing the formation of monodisperse particles in the specified size regime.

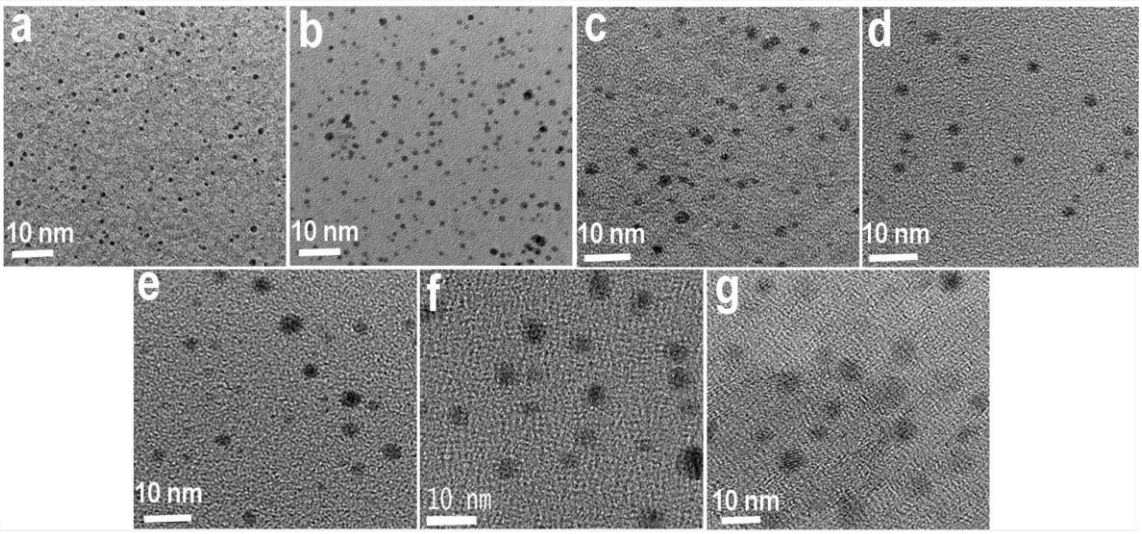

Figure 3.2. (a-g) TEM images of the PVP-stabilized gold nanoparticles corresponding to sets A-G respectively.

3.1.3.3. Aggregation amongst the Ultrasmall Gold Particles

Now, two different methodologies were adopted in pursuing aggregation amongst the as-synthesized gold nanoparticles and the measurement of the UV-vis extinction spectra was performed to enlight the aggregation mechanism.

3.1.3.3.1. Spontaneous Aggregation

The as-synthesized gold nanoparticles were allowed to aggregate by keeping the colloidal gold (0.5 mM) undisturbed at room temperature (298±5 K) in a closed vial for about 45 hrs. Figure 3.3A represents the evolution of surface plasmon band of the aggregates of gold nanoparticles (set A). It is observed that, although, the monodispersed gold nanoparticles do not exhibit any significant surface plasmon band, upon ageing with time, a distinct and broad surface plasmon band evolves at around 520 nm. It is noticeable that there is no red shifting of the plasmon band which is, usually, observed upon aggregation of the large particles. This is, probably, due to the fact that aggregation of the ultrasmall gold particles forms nanoparticle cluster and collectively induce the surface plasmon oscillation that oscillate with a characteristic wavelength of light on coupling with the incident electromagnetic radiation field.[36] Polymer-stabilized gold nanoparticles experience Brownian encounters to cause aggregation of the nanoparticles upon ageing.[37] Moreover, in the present experiment, the particle sizes are very small and as a result, the

surface energy of the particles is very high. Therefore, due to Brownian encounters of the nanoparticle sols and high surface energy, PVP-stabilized small gold nanoparticles are prone to aggregation under ubiquitous condition. Therefore, a distinct SPR band appears at the wavelength around 520 nm and the absorbance increases with successive increase of the time of elapse for the gold nanoparticle assemblies. Figure 3.3B shows the UV-vis spectra of seven different sizes of gold nanoparticles upon spontaneous aggregation

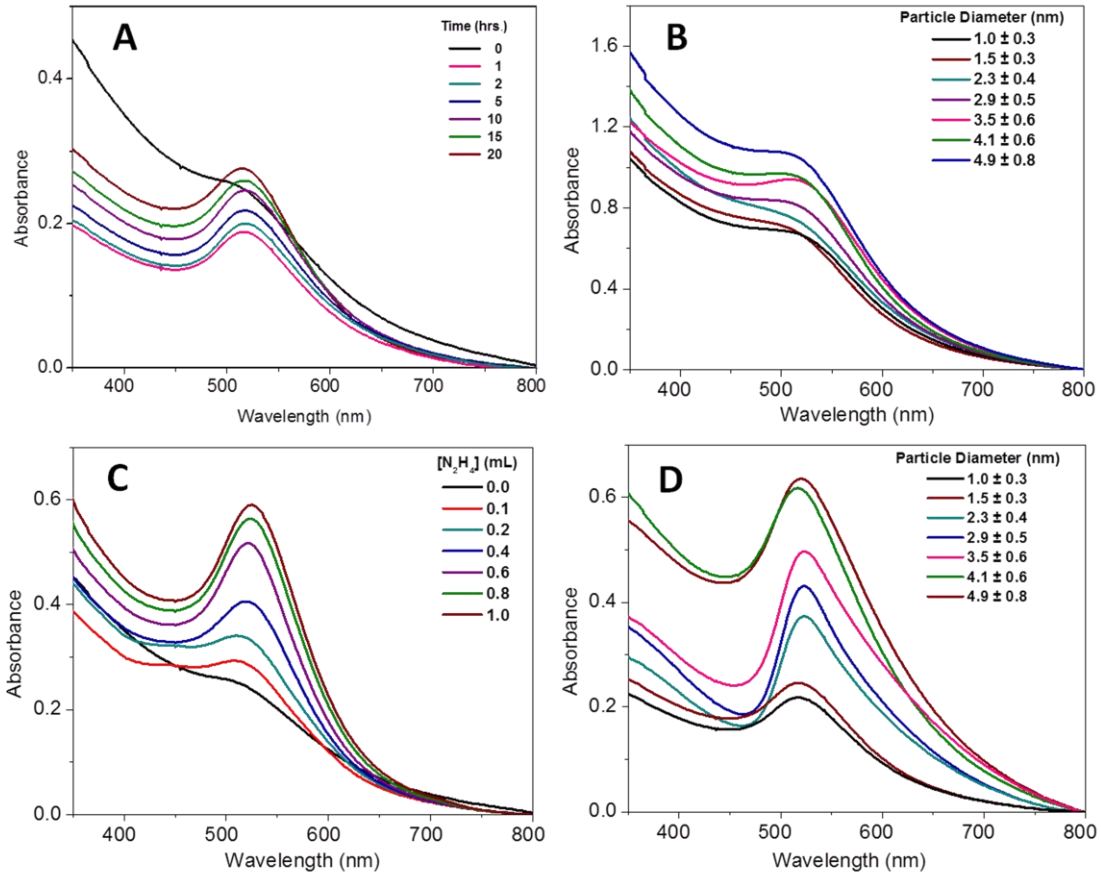

Figure 3.3. (A) Evolution of surface plasmon band of gold nanoparticles (set A) upon spontaneous aggregation at different time intervals and (B) UV-vis spectra of seven different sizes of gold nanoparticles upon spontaneous aggregation followed after 45 hrs. for each set of gold nanoparticles; (C) Evolution of surface plasmon band of gold nanoparticles (set A) upon induced aggregation at different concentrations of hydrazine and (D) UV-vis spectra of seven different sizes of gold nanoparticles upon induced aggregation measured after addition of 1.0 mL of hydrazine in each set of gold nanoparticles.

followed after 45 hrs. of the synthesis of the particles (0.5 mM). It is seen that the absorbance gradually increases without significant red shift of the absorption maximum with increase in size of the individual gold particles in the aggregate as has been predicted theoretically by Gedanken and co-workers.[38]

3.1.3.3.2. (Hydrazine)-Induced Aggregation

The gold nanoparticles were also aggregated induced by hydrazine and the color changes slowly from bright brown to red and subsequently to violet. Hydrazine was chosen for aggregation of the gold particles because of its structural simplicity and to avoid any complicacy for further fluorescence experiments. Figure 3.3C presents the evolution of surface plasmon band due to aggregation of the gold nanoparticles (0.5 mM, set A) upon addition of different concentrations of hydrazine. It is observed that, although, the monodispersed gold nanoparticles do not exhibit any significant surface plasmon band, upon addition of hydrazine, a distinct and broad surface plasmon band evolves at around 520 nm.[39] It is also seen that SPR band is sharpened with concomitant increase in absorbance when the concentration of hydrazine gradually increases. Upon addition of hydrazine to PVP-stabilized gold nanoparticles, the particles are aggregated due to the screening of electrostatic repulsion (despite the presence of steric repulsion) between the particles and consequently, the absorption spectrum is modified. When the size of the gold nanoparticles decreases, the electronegativity of gold nanoparticles increases and as a result, smaller gold nanoparticles have higher affinity to accept electrons. On the other hand, hydrazine is a Lewis base and can donate lone pair of electrons to the gold nanoparticles. Since each hydrazine molecule has two nitrogen atoms, it can act as a bridge or linker between the two nanoparticles in linear fashion by donating lone pair electrons. We have also tried to induce aggregation of gold nanoparticles by adding other nitrogen containing Lewis bases, ammonia or pyridine, but there is no aggregation between the particles. This observation strongly supports that the hydrazine molecules act as a linker between gold nanoparticles in inducing aggregation and the extent of aggregation become stronger with increasing concentration of hydrazine to the gold nanoparticles. Figure 3.3D shows the UV-vis spectra of seven different sizes of gold nanoparticle (0.5 mM) aggregates produced upon addition of 1.0 mL of hydrazine in each

set of the particles. It is observed that the absorbance gradually increases without significant red shift of the absorption maximum with increase in size of the individual gold particles in the aggregates.

3.1.3.3.3. Comparative Overview between Spontaneous and Induced Aggregation

Now, let us have a comparative overview between the spontaneous and induced-aggregated gold nanoparticles. In the spontaneous aggregation, the absorption spectrum is broad indicating the formation of aggregated structures with 'loose affiliation' of the particles.[40] In this aggregation process, the driving force of aggregation is the high surface energy of the ultrasmall particles. Therefore, it is very difficult to miniature the aggregated state and may be referred to as 'thermodynamically controlled aggregation'.[41] On the other hand, upon hydrazine-induced aggregation, the spectrum appears at 520 nm and less broadened that arises in case of relatively larger sized nanoparticles, indicating the formation of 'compact association' of the ultrasmall particles.[42] In this aggregation process, control of aggregation could be achieved through addition of hydrazine, a Lewis base, which acts as a linker between the particles. Therefore, the driving force of aggregation is much higher than the spontaneous aggregation leading to compact packing of the nanoparticles and could be assumed as 'kinetically controlled aggregation'. The TEM images of the spontaneously and induced-aggregated gold nanoparticles (set G) are shown in Figure 3.4.

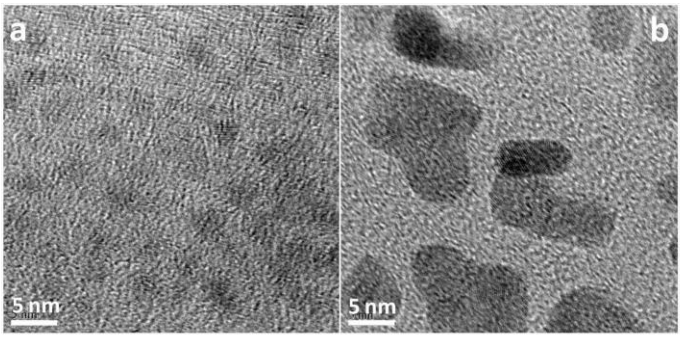

Figure 3.4. TEM images of the gold nanoparticle (sets G) aggregates arising due to (A) spontaneous and (B) induced aggregation.

3.1.3.4. Fluorescence Spectra of FITC in the Presence of Spontaneous and Induced-Aggregated Gold Nanoparticles

Now, we have employed fluorescein isothiocyanate as a molecular probe to monitor the characteristic features of spontaneously and induced-aggregated gold nanoparticles. It

has been seen that the fluorescence spectrum of FITC is not affected, appreciably, by the addition hydrazine in the experimental concentration range. The pH of the spontaneous and induced aggregated gold nanoparticles is, approximately, 7.5 and 10.0; but to measure the fluorescence emission, the pH was adjusted to ~8.0 for all sets including pure FITC. It was noted that, in acidic pH range, fluorescence intensity of FITC molecules is lower as compared to alkaline condition. Fluorescence intensity of FITC, in alkaline condition, almost remains invariant with respect to change of pH. Performing the experiments either in acidic (pH~3.0 to 6.5) or highly alkaline conditions (pH~ 10.0 to 13.0), the binding of FITC molecules on the gold nanoparticle surface decreases that gives rise to additional complexity to the sensitivity of the experiment. Therefore, the pH of the solution was adjusted to ~8.0 and does not change, considerably, in the different sets of experiments for fluorescence measurements. Fluorescein isothiocyanate molecules have electron enriched isothiocyanate group (-N=C=S) and in particular, containing lone pair of electrons on larger sulfur atom. Therefore, the dye molecules can donate electrons via polarizable sulfur atoms onto the gold nanoparticles and eventually, a fraction of FITC molecules become attached onto the surface of the particles. At this pH, FITC exists in anionic form and the binding occurs through the sulfur atom of reactive isothiocyanate group onto the surface of gold particles.[43]

3.1.3.4.1. Aggregates containing Gold Nanoparticles of Different Sizes

Figure 3.5 shows the fluorescence spectra of FITC (40 nM) in the presence of spontaneously and induced-aggregated gold nanoparticles (1 μM) of variable sizes. In the present experiment, quite dilute solutions have been used so as to minimize the effects of the absorption of excitation light and re-absorption of molecular fluorescence light due to the presence of the gold nanoparticles as well as the near field effects on the absorption cross section (so-called ‘‘trivial effects’’). It is seen that there is enhancement of fluorescence of FITC molecules in the presence of both spontaneous and induced-aggregated gold nanoparticles. It was observed that the aggregates, themselves, as well as the individual gold nanoparticles are non-fluorescent. However, when the individual gold nanoparticles, prior to aggregation, were added to the FITC solution, quenching of fluorescence was observed.

Metallic nanostructures modify the intrinsic photophysical characteristics of fluorophores when the probe molecules are placed near the metal surface. In the presence of isolated metal nanoparticles, fluorescence is quenched due to electron and energy transfer processes from the dye molecules to the nanoparticulate systems.[44] However, in the presence of electromagnetically coupled aggregated metal clusters, the radiative decay rates and the quantum yield of the fluorescent species may increase significantly.[45] According to the model proposed by Weitz et al.,[24] the scattering intensity ratio for fluorescence of adsorbed molecules on the metal surface to that of the free ones is given by,

$$R_{fluo} = |A(\omega_L)|^2 |E_L|^2 \frac{\Gamma_0}{\Gamma_0 + \Gamma_0^s} \quad (3.1)$$

where, E_L is local electric field at the molecule due to the incident beam. The amplification factor, $A(\omega_L)$ is increased local field intensity through the excitation of

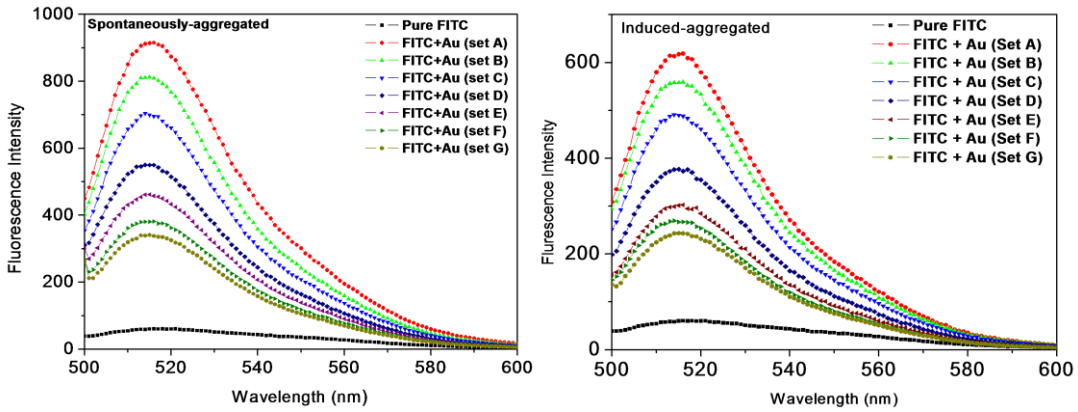

Figure 3.5. Fluorescence spectra of FITC molecules in the presence of (a) spontaneously and (b) induced-aggregated gold aggregates containing different particle sizes after 1 min. of the preparation of solution.

electronic plasmon resonances governed by the morphology and dielectric properties of the nanoparticles. The parameters, Γ_0 denotes the radiative and non-radiative transition rate from excited state to the ground state for free molecules while Γ_0^s is taken to represent an average value of the surface-induced decay rate for molecules on the gold nanoparticles. The origin of the significant fluorescence enhancement near nanostructured metal can be understood by the consideration of two contributing factors.

Firstly, by concentrating the incident light into local density of states, so-called electromagnetic 'hot spots' (i. e., their associated electric fields ($|E|/|E_0|$ where $E = E_0E_L$) are stronger and more localized in the gaps between the particles),[46] surface plasmon excitation of nanostructured metallic surfaces can lead to increase absorption of the surrounding fluorophores by the incident light.[47] Secondly, metal nanostructures alter the radiative and the non-radiative decay rates of the neighbouring fluorophores by changing both the fluorescence lifetime and quantum yield of the emitter and hence, plasmonic nanostructures can be used as nanoantenna.[48] The resultant balance of these processes leads to enhancement of molecular fluorescence and the measured enhancement impact important spectroscopic consequences.

Figure 3.6. shows the relative enhancement of fluorescence with increase in size of the gold nanoparticles in the aggregates. It is seen that the enhancement efficiency decreases with increase in size of the gold nanoparticles within the aggregates. However, the salient feature of physical significance is that the relative fluorescence is distinctly different in the two different size regime of the particles.

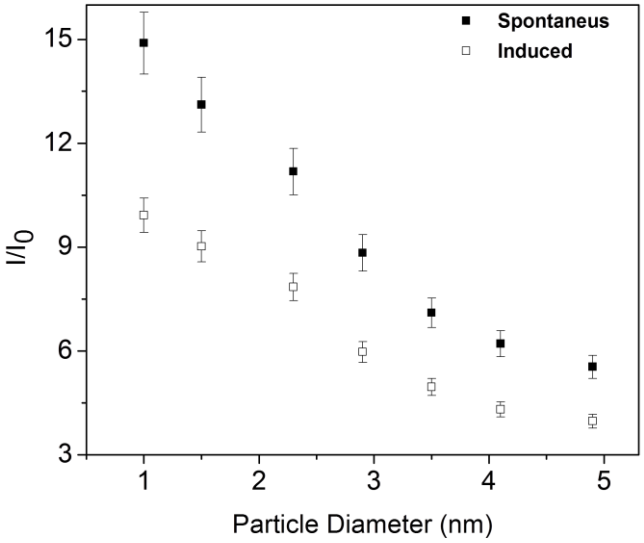

Figure 3.6. Relative fluorescence enhancement of FITC molecules in the presence of (a) spontaneously and (b) induced aggregated gold nanoparticles of different sizes after 1 min. of the preparation of solution.

The enhancement efficiency in the presence of different sizes of gold nanoparticles could be treated by considering the effect of nanoparticle size on the aggregates of the particles. It is plausible that with increase in size of the particles, the interstitial space increases and the number of neighboring clusters surrounding the electromagnetic 'hot spot' decreases.[48] Due to decrease in the number of clusters surrounding the electromagnetic 'hot spot', the electromagnetic field enhancement effect on the dye molecules decreases and the enhancement efficiency gradually decreases.[49] The different sizes of the particles

in the aggregate produce characteristic patterns and shifts in LSPR resonances, which lead to different wavelength-dependent local field enhancement factors at the absorption and emission frequencies of the dye.[50] However, the dramatic change in the enhancement efficiency in the presence of very small sizes of the nanoparticles could be accounted by considering that is dependent on the core size and there is a transition at 2.3 nm due to the emergence of optical gap between the highest occupied and lowest unoccupied orbitals.[51] When ultrasmall gold particles (those do not possess any surface plasmon band) are coupled together, it is not expected to show significant changes upon aggregation and the clustered aggregates can exhibit properties similar to the one observed for larger particles (diameter > 5 nm).[36] The absorption arises from the surface plasmon oscillation modes of conduction electrons in the clustering of these small gold nanoparticles that collectively can induce the surface plasmon resonance. Upon aggregation, the individuality of the clusters is maintained by (arbitrarily) thin separating layers between the neighboring clusters and the clusters remain polarizable individuals even after aggregation.[52] The integrated total extinction due to all clusters hit by the light beam is given by the sum-over all aggregate spectra weighed by the size distribution. After the critical size of 2.3 nm, the individual particles within the aggregate can lead to quenching of fluorescence of the probe molecules vis-a-vis the aggregation leading to enhancement of fluorescence and in consequence, the enhancement is predominating over the quenching of fluorescence of the probe molecules.

3.1.3.4.2. Different Concentration of the Aggregates

Figure 3.7 shows the fluorescence spectra of FITC (40 nM) in the presence of spontaneously and induced-aggregated gold nanoparticles (set A) of different concentrations. It is seen that there is enhancement of fluorescence of FITC molecules in the presence of both spontaneous and induced-aggregated gold nanoparticles.

The relative fluorescence intensity of FITC in the presence of different concentrations of spontaneous and induced-aggregated gold nanoparticles (set A) is shown in Figure 3.8. It is also observed that, initially, the fluorescence intensity of FITC gradually increases with increase in concentration of aggregated gold nanoparticles; at a particular concentration, it reaches the optimal and then, becomes constant. It has also been noted

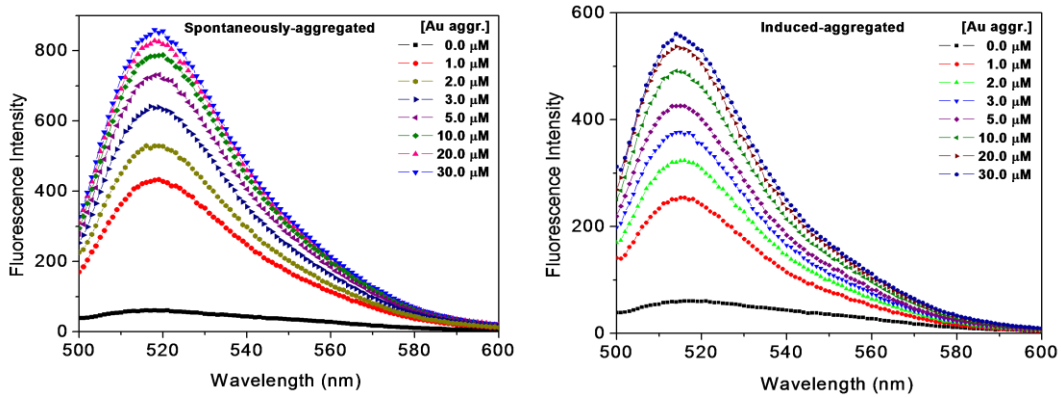

Figure 3.7. Fluorescence spectra of FITC molecules in the presence of different concentrations of (a) spontaneously and (b) induced aggregated gold aggregates containing gold nanoparticles (sets A) after 1 min. of the preparation of solution.

that the maximum enhancement occurs towards the higher concentration with increase in size of the particles in the aggregate.

In the absence of nanoparticles, the fluorophores radiate into free space. The presence of nearby metallic surfaces or particles can alter the free-space condition. Under this situation, in the definition of fluorescence quantum yield, φ_f, a further factor, k appears. According to Parker,[53] fluorescence intensity (I) is proportional to the concentration of the fluorophore as given by,

$$I = I_0 \varepsilon c l \varphi_f k \qquad (3.2)$$

where, I_0 is the intensity of the exciting source beam, ε the molar absorption co-efficient of the fluorescent probe, c its concentration, l the path length of the sample, φ_f its quantum yield and k a geometrical factor that accounts for the geometry of the optical system. The quantities involved within k are the mutual polarization effect among all the components, *viz.*, fluorophore and nanoparticles, fluorophore and solvent, nanoparticles and solvents, and nanoparticles among themselves when the particles are electromagnetically coupled, yielding optical properties that are not the simple sum of those of the individual particles. The metal could be considered as a continuous dielectric characterized by the experimental optical constant.[54] It is well known that the plasmonic properties determining the final enhancement or quenching of the fluorescence depend not only on the characteristics of the nanoparticles (its nature, size, shape, interparticle

distance and the local dielectric properties) but also on the position and orientation of the fluorophore with respect to the nanoparticulate systems.[55,56] Coupling of all these environmental and structural parameters does not necessarily present an additive character and the separation of the explicit contribution of each component is extremely difficult.[57] Such an interpretation is very delicate as the final net response of the probe molecules near the nanoparticle surface is determined by the coupling of all these components.[58] In the present experiment, it is seen that with increase in concentration of the gold nanoparticle aggregates, the enhancement efficiency is linear with increase in concentration of the gold nanoparticle aggregates. Therefore, it can be concluded that the aggregates are isotropic in nature for a particular size of the gold nanoparticles.

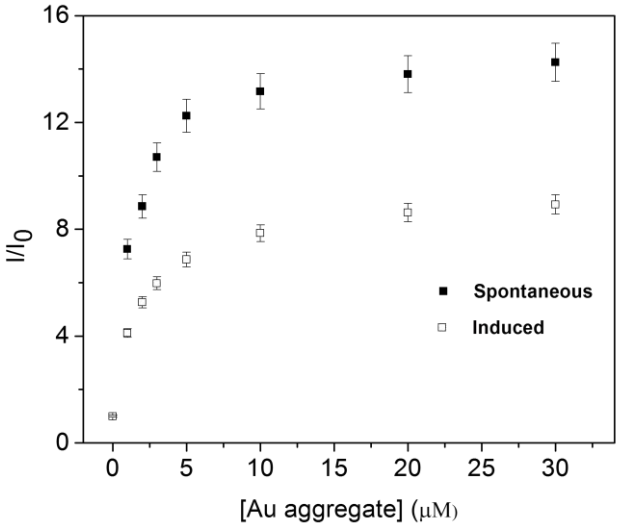

Figure 3.8. Relative fluorescence enhancement of FITC molecules in the presence of (a) spontaneously and (b) induced aggregated gold nanoparticles of different sizes after 1 min. of the preparation of solution.

3.1.3.4.3. Different Time of Interaction

The fluorescence spectra of FITC molecules (40 nM) in presence of both spontaneous and induced-aggregated gold nanoparticles (1 μM) have been measured as a function of time of ageing the solution (Figure 3.9.). It is seen that there is a huge enhancement of fluorescence just after addition of the dye to the gold nanoparticle aggregates in case of spontaneous aggregation and then, successively decreases while there is hardly any change in case of induced aggregated gold nanoparticles. Interestingly, it has been observed that the measured fluorescence signal, decreases exponentially with time for spontaneously aggregated gold nanoparticles, while almost remains same for induced-aggregated gold (set A) as shown in Figure 3.10A. This is due to the fact that, during

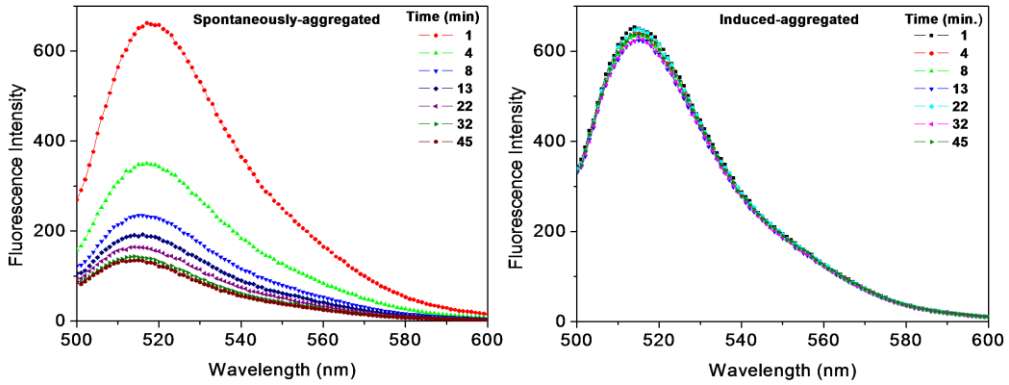

Figure 3.9. Fluorescence spectra of FITC molecules in the presence of (a) spontaneously and (b) induced aggregated gold aggregates containing gold nanoparticles (sets A) at different time intervals.

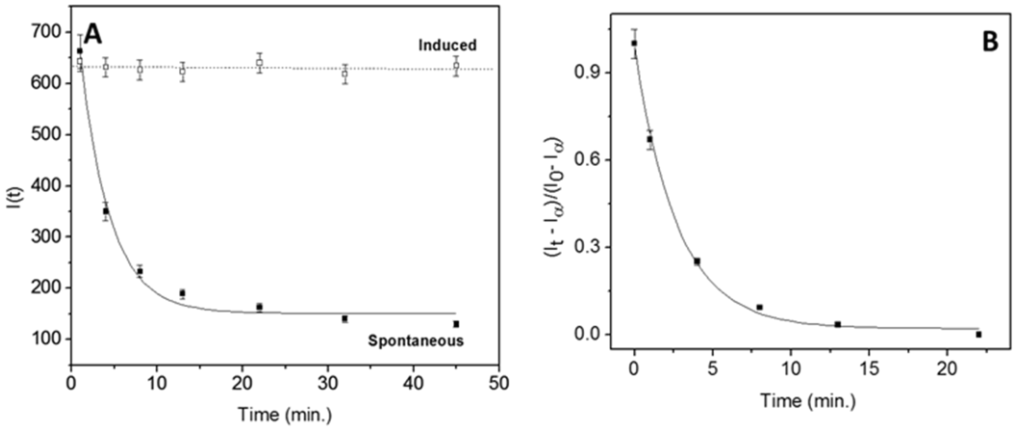

Figure 3.10. (A) Fluorescence intensity of FITC molecules at different time intervals in the presence of (a) spontaneously and (b) induced aggregated gold aggregates containing gold nanoparticles (sets A) and (B) first order analysis of the curve in the presence of spontaneously gold nanoparticles.

colloid aggregation, the evolution of mean aggregate size as a function of time bears an exponential growth as P(t) ~ exp (t/k), k is a time constant.[59] Figure. 3. 10B shows that the interaction of the probe molecules with gold nanoparticle aggregates in solution could be fitted, reasonably, well by first order rate equation,[60]

$$\left(\frac{I_t - I_\infty}{I_0 - I_\infty}\right) = e^{-k_a t} \qquad (3.3)$$

where, k_a is the association rate of the dye molecules to the nanoparticles, t the time, I_0 the fluorescence signal at time $t = 0$ and I_∞ the signal when fluorescence no longer

changes with time. These phenomena could be accounted by assuming that the packing of the particles in spontaneously aggregated gold nanoparticles are not in ordered arrangement probably for weak interaction force (surface energy) which is the driving force for aggregation. Since the packing as well as particle arrangement are not in proper order, result less enhancement in local field intensity, i. e., the effectiveness of hot spots decreases, which results the less number of molecules in the excited state and therefore, intensity decreases but not less than the pure FITC molecules with time. However, in induced aggregated gold nanoparticles, the hydrazine molecules by kinetically controlled process renders the particles to be organized in proper arrangement. After addition of FITC molecules, the molecules are incorporated inside the electromagnetic 'hot spots' and there is no possibility to change the packing of the nanoparticle aggregates. So, the aggregated particles and therefore, fluorescence enhancement almost remain same for induced-aggregated gold nanoparticles with time. The plausible binding modes of the dye molecules to the spontaneous and induced-aggregated gold nanoparticles are shown in Scheme 3.2.

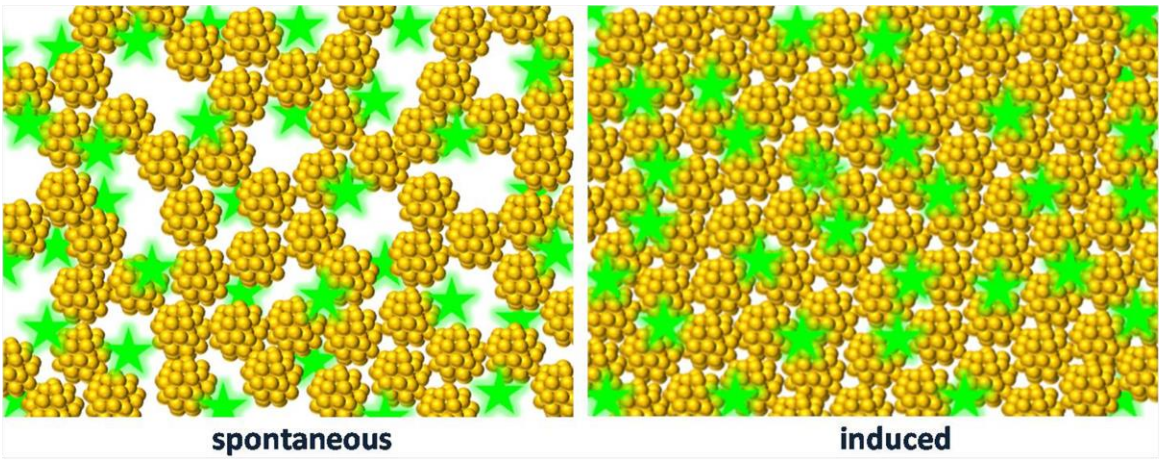

Scheme 3.2. Schematic presentation of the plausible binding modes of the dye molecules to the (A) spontaneous and (B) induced-aggregated gold nanoparticles.

3.1.4. Conclusion

In conclusion, fluorescence spectroscopy has been employed in realizing the physicochemical insights of aggregation phenomenon of the size-selective gold nanoparticles undergoing spontaneous and induced-aggregation under stipulated conditions. It is seen that there is enhancement of fluorescence intensity of FITC in the presence of both spontaneous and induced-aggregated gold nanoclusters. It is observed that the fluorescence sensitivity is able to distinguish seven different sizes of the gold nanoparticle aggregates and maximum enhancement of intensity arises at higher concentration with increase in size of gold particles within the aggregates. However, the salient feature of physical significance is that the maximum enhancement of intensity with time has remained same for induced-aggregated gold while decreases exponentially with spontaneously aggregated gold particles. The enhancement of the molecular fluorescence increases the molecular detection efficiency by amplifying/tailoring the electromagnetic radiation field of the neighboring fluorophores near metal nanoparticles.

3.2. Critical Point of Relaying from Nanosurface Energy Transfer to Förster Resonance Energy Transfer

3.2.1. Introduction

The interaction of fluorescent molecules with metallic nanoparticles is complex and can lead to excited state enhancement[29, 61, 62] or quenching.[18, 24] Many attempts have been made to explain the observed quenching when in close proximity to the metal surface; however, no such single model has been capable of explaining the observations. Since the pioneering theoretical investigation by Rupin in 1982, it has been established that the total decay rate of an excited molecule near a small sphere is governed by radiative loss through the modification of the boundary conditions of the electromagnetic field and non-radiative decay through which energy is dissipated.[63] While a donor molecule is placed in the vicinity of a metallic nanostructure, not only resonant energy transfer takes place but also the radiative lifetime of the donor molecule changes. Resonant energy transfer (RET) systems, consisting of organic dye molecules and noble metal nanoparticles, have received considerable interest in designing synthetic light harvesting systems or as a spectroscopic ruler for tracking biomolecular conformational changes, drug discovery, and cellular imaging.[64] Förster theory has, successfully, been applied to describe the dynamics of RET by invoking the Fermi Golden Rule (GR) in the dipole approximation of energy transfer and the weak coupling approximation, according to which the electronic interaction between the molecules is small in comparison to the coupling to the bath i. e., hot transfer and/or memory effects are neglected which means that intermolecular interaction is negligible in comparison to nanoparticle-fluoroprobe interaction.[63] The Golden Rule approximation relates the energy transfer rate (k_{EnT}) to a product of the interaction elements of the donor (F_D) and acceptor (F_A), $k_{EnT} \sim F_D F_A$. These interaction elements can be simplified such that their separation distance (d) dependencies are sole functions of their geometric arrangement. For single dipoles, $F \sim 1/d^3$, for a 2D dipole array, $F \sim 1/d$, and for a 3D dipole array, $F = constant$ such that the power of the distance factor decreases as the dimension increases.[65] Förster resonance energy transfer (FRET), in which excitation energy of the donor is transferred to the acceptor *via* an induced-dipole–induced-dipole interaction, is easily derived from this

rule, such that, $k_{FRET} \sim F_D F_A \sim (1/d^3)(1/d^3) \sim 1/d^6$ and in practice, commonly, expressed as $k_{FRET} = (1/\tau_D)(R_0/R)$.[6] The Förster radius (R_0) is a function of the oscillator strengths of the donor and acceptor molecules, their mutual energetic resonance, and the vector addition of their dipoles. Thus, FRET is a spectroscopic technique in which excitation energy of the donor is transferred to the acceptor *via* an induced-dipole–induced-dipole interaction. Although FRET technology is very sensitive to the distance between the donor and an acceptor and can, routinely, be applied at the single-molecule detection limit, the nature of the dipole-dipole mechanism, effectively, constrains the length scales in FRET-based methods that have detectable distances limited to <100 Å. On the other hand, nanomaterial surface energy transfer (NSET) is dipole-surface type energy transfer from a molecular dipole to a nanometal surface, such that, $k_{NSET} \sim F_D F_A \sim (1/d^3)(1/d) \sim 1/d^4$ and in practice, commonly, expressed as $k_{NSET} = (1/\tau_D)(R_0/R)^4$. Thus, NSET is an efficient quenching technique capable of measuring distances more than doubles the traditional Förster range (220 Å).[66]

Förster resonance energy transfer (FRET) involves the nonradiative transfer of excitation energy from an excited donor, D, (after absorption of a higher energy photon) to a ground-state acceptor, A, brought in close proximity, which can radiatively emit a lower energy photon.[67] FRET processes are driven by dipole–dipole interactions and depend on the degree of spectral overlap between donor photoluminescence and acceptor absorption, and on the sixth power of the separation distance between the donor and acceptor pair.[68] According to Förster theory,[67] the rate of energy transfer is given by,

$$k_{DA} = \frac{B \times Q_D I}{\tau_D r^6} = \left(\frac{1}{\tau_D}\right) \times \left(\frac{R_0}{r}\right)^6 \qquad (3.4)$$

where, τ_D is the excited-state radiative lifetime of the donor and R_0 is the Förster separation distance corresponding to a rate of FRET equaling the rate of radiative decay ($k_{DA} = 1/\tau_D$). R_0 is a function of the refractive index of the medium, η_D; Avogadro number, N_A; the donor PL quantum yield, Q_D ; the overlap integral, $J(\lambda)$; and a parameter, k_p, that depends on the relative orientation of the donor and acceptor dipoles. Förster distance is defined as the distance at which the transfer rate $k_t(r)$ is equal to the decay rate of the donor in absence of the acceptor. The Förster distance (R_0) is represented as,[69]

$$R_0 = \left(\frac{9000(\ln 10)\kappa_p^2 Q_D}{N_A 128\pi^5 \eta_D^4} J(\lambda) \right)^{1/6} \quad (3.5)$$

where,Q_D is the quantum yield of donor in absence of acceptor, η is the refractive index of the medium, k^2 is the orientation factor of two dipoles interacting and is usually assumed to be equal to 2/3, and $J(\lambda)$ is the overlap integral between donor emission and acceptor absorption spectra. In simplified form, the Förster distance can be written as,

$$R_0 = 9.78 \times 10^3 [k^2 \eta^{-4} Q_D J(\lambda)]^{1/6} \quad \text{(in angstroms)} \quad (3.6)$$

For NSET, however, R_0 can be calculated independently using Persson-Lang model[65]

$$R_0 = \left\{ \frac{0.225\phi_D}{\omega_D^2 \omega_F k_F} C^3 \right\}^{1/4} \quad (3.7)$$

where, c is the speed of light, Φ_D is the quantum yield of the donor in the absence of the acceptor, ω_D is the angular frequency for the donor (3.43×10^{15} s^{-1}), ω_F is the angular frequency of the bulk gold (8.4×10^{15} s^{-1}) and k_F is the Fermi wave vector for bulk gold (1.2×10^8 cm^{-1}).[70]

In this sub-section, we have made an effort to realize an experimental demonstration of the different energy transfer processes (FRET and NSET) between the fluoroprobe and the gold nanoparticles. Gold nanoparticles of variable sizes (1–55 nm) have been synthesized using sodium borohydride as reducing agent and poly(N-vinyl 2-pyrrolidone) (PVP) used as the capping agent and/or citrate as reducing and capping agent. The synthesized gold nanoparticles have been characterized by UV-vis spectroscopy and transmission electron microscopy. Then, fluorescent dye molecule containing high quantum yield, fluorescencein isothiocyanate (FITC) has been employed as molecular probe in understanding the physical principles of surface behavior of gold nanoparticles of variable sizes and thereafter, to validate the experimental results in the light of NSET and FRET mechanism.

3.2.2. Experimental

3.2.2.1. Synthesis of Gold Nanoparticles of Variable Sizes

Monodisperse gold clusters of variable sizes ranging from 1 to 5 nm have been synthesized by following the method reported by Tsukuda and co-workers.[32] In a typical

procedure, an aqueous solution of $HAuCl_4.3H_2O$ was mixed with PVP in different molar ratio (R) and reduced with sodium borohydride for the synthesis of different sets of gold nanoparticles. Firstly, an aqueous solution (20 mL) of requisite amount of PVP (5–100 mM) was stirred for 2 h on an ice-bath maintained at 0 ^{0}C. Subsequently, an aliquot of $HAuCl_4.3H_2O$ (0.5 mM) solution was added and the mixture was stirred for 1 h. Then, ice-cold aqueous solution of $NaBH_4$ (0.1 M, 2 mL) was added instantaneously into the mixture under vigorous stirring. The color of the mixture immediately turned from pale yellow to bright brown indicating the formation of small gold nanoparticles. The stirring was continued for another half an hour. The particles are stable for a couple of days while stored in the freeze. The variation in synthetic conditions and sizes for different sets of gold particles are summarized in Table 3.2.

Table 3.2. Synthetic Conditions and Characteristic Parameters of the Different Sets of Gold Particles

Set	[$HAuCl_4$] (mM)	[PVP] (mM)	R= [PVP]/[$HAuCl_4$]	Colour	Avg. diameter (nm)
A	0.5	100.0	200	brown	1.0±0.2
B	0.5	85.0	170	brown	1.3±0.3
C	0.5	75.0	150	brown	1.6±0.3
D	0.5	50.0	100	brown	2.2±0.4
E	0.5	37.5	75	brown	2.7±0.5
F	0.5	25.0	50	brown	3.5±0.6
G	0.5	12.5	25	brown	4.1±0.6
H	0.5	5.0	10	brown	4.9±0.8

[#]For gold nanoparticle synthesis, the total volume of the solution was 25 mL.

The monodispersed gold nanoparticles of different size ranges have been synthesized following the methods reported by Tsukuda et al.[71] In this method, 5 to 8 nm gold particles have been synthesized by reduction of $HAuCl_4.3H_2O$ by Na_2SO_3 followed by the addition of cluster of Au seeds of sizes 1.3±0.3 nm stabilized by PVP. Two different sets of gold nanoparticles have been prepared, by changing the ratio of growth solution of precursor gold to gold seeds as 1:9, one basified with K_2CO_3 (Set I) and the other at neutral conditions (Set J) under N_2 atmosphere and dialyzed by centrifugal ultrafiltration.

For achieving monodispersed gold colloids of 8 to 55 nm sized particles, well-documented Frens method[72] has been employed in which trisodium citrate has been used as the surface capping as well as reducing agent. In this typical method, 50 mL aqueous solution of $HAuCl_4.3H_2O$ (0.25 mM) is heated to boiling and 2.0, 1.6, 1.3, 1.0, 0.875,

Table 3.3. Synthetic Conditions[#] and Characteristic Parameters of the Size-Specific Gold Nanoparticles

Set	Amount of $HAuCl_4$ solution (10 mM, mL)	Amount of trisodium citrate solution (1%, mL)	Colour	λ_{max} (nm)	Diameter (nm)
K	1.25	2.0	dark red	518	8.0 ± 1.5
L	1.25	1.6	red	519	10.0 ± 1.5
M	1.25	1.3	red	520	13.0 ± 2.0
N	1.25	1.0	red	522	16.0 ± 2.5
O	1.25	0.875	red	523	20.0 ± 3.0
P	1.25	0.625	red	528	32.0 ± 4.0
Q	1.25	0.400	pink	533	55.0 ± 5.0

[#]Total volume of the solution was maintained to 50 mL.

0.625 and 0.4 mL of trisodium citrate (1%) have been added for different sets. At about 25 s, the colour of the boiling solution turns faintly blue which, consequently, changes into a brilliant red at about 70 s indicating the formation of gold nanoparticles. Then, the colloidal gold solutions are cooled to room temperature and functionalized with PVP (50 mM) by stirring for 3 h. The variation of size and the synthetic conditions have been summarized in figure Table 3.3.

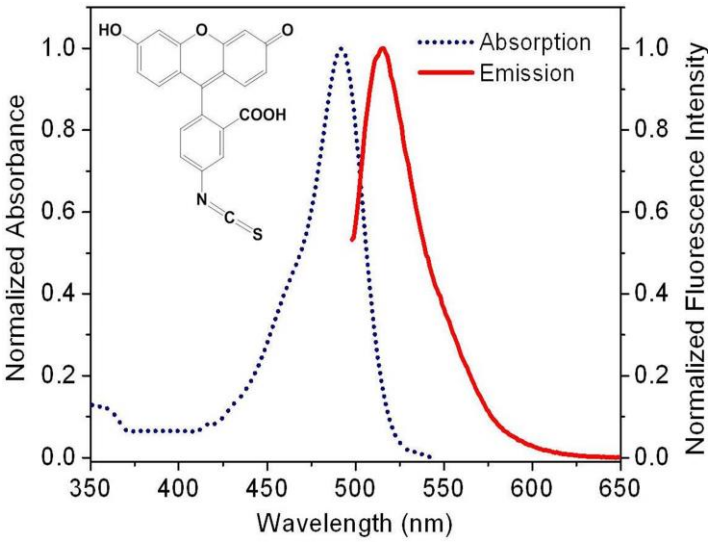

Figure 3.11. Absorption and emission spectra of FITC molecules in aqueous solution. Inset shows the molecular structure of dye molecules.

3.2.3. Results and Discussion

Fluorescein isothiocyanate (pK_a ~ 6.7) belonging to hydroxyxanthene dyes and is known for their strong absorption (λ_{abs}~ 492 nm; extinction co-efficient >70,000 $M^{-1}cm^{-1}$) and emission (λ_{em}~ 516 nm; φ_f ~ 0.95) in the visible region.[33] It is widely used as a fluorescent tracer in many applications, such as, in microscopy, in a type of dye laser as the gain medium, in forensic and serology to detect latent blood stains and as a bio-tagger to elucidate the cellular transport processes.[34] The absorption and emission spectra of FITC molecule are shown in Figure 3.11. The molecular structure of the dye is shown in the inset.[43]

The gold particles have been characterized by UV-vis spectroscopy as shown in Figure 3.12. It is seen that the gold particles do not exhibit any prominent surface plasmon band in the visible region instead indicating a signature of SPR at about 520 nm representing the formation of ultra-small gold collective oscillation of the conduction electrons on the metal surface with electromagnetic radiation, so called surface plasmon has not been exhibited, due to extremely small sizes of the gold nanoparticles. On increasing the size of the gold nanoparticles in the range of 5 - 55 nm the surface plasmon band become prominent, broadened and shifted to the red.[73] Moreover, it is well-established that the absorbance of the surface plasmon band increases with increasing size of the gold nanoparticles.[74] From the transmission electron micrographs, it is seen that the gold nanoparticles are spherical or nearly spherical with average diameter 1.0 ± 0.2 (A), 1.3 ± 0.3 (B), 1.6 ±0.3 (C) 2.2 ±

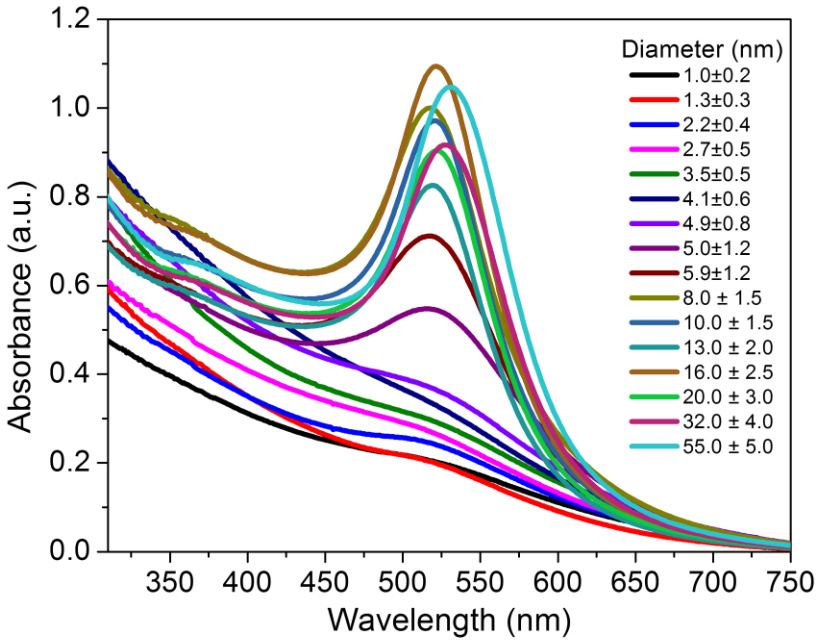

Figure 3.12. Absorption spectra of gold nanoparticles of variable sizes of 1 to 55 nm.

0.4 (D), 2.7 ± 0.5 (E), 3.5 ± 0.6 (F), 4.1 ± 0.6 (G) 4.9 ± 0.8 (H) 5.0 ± 1.0 (I), 6 ±1.5 (J), 8±1.5 (K), 10 ±1.5 (L), 13 ± 2.0 (M), 16 ± 2.5 (N), 20 ±3.0 (O), 32 ± 4.0 (P) and 55 ± 5.0 (Q) nm, respectively. Figure 3.13 shows the representative TEM images of sets A, B, E, F, I, L, M, N and O respectively, showing the monodispersed particles in the respective region.

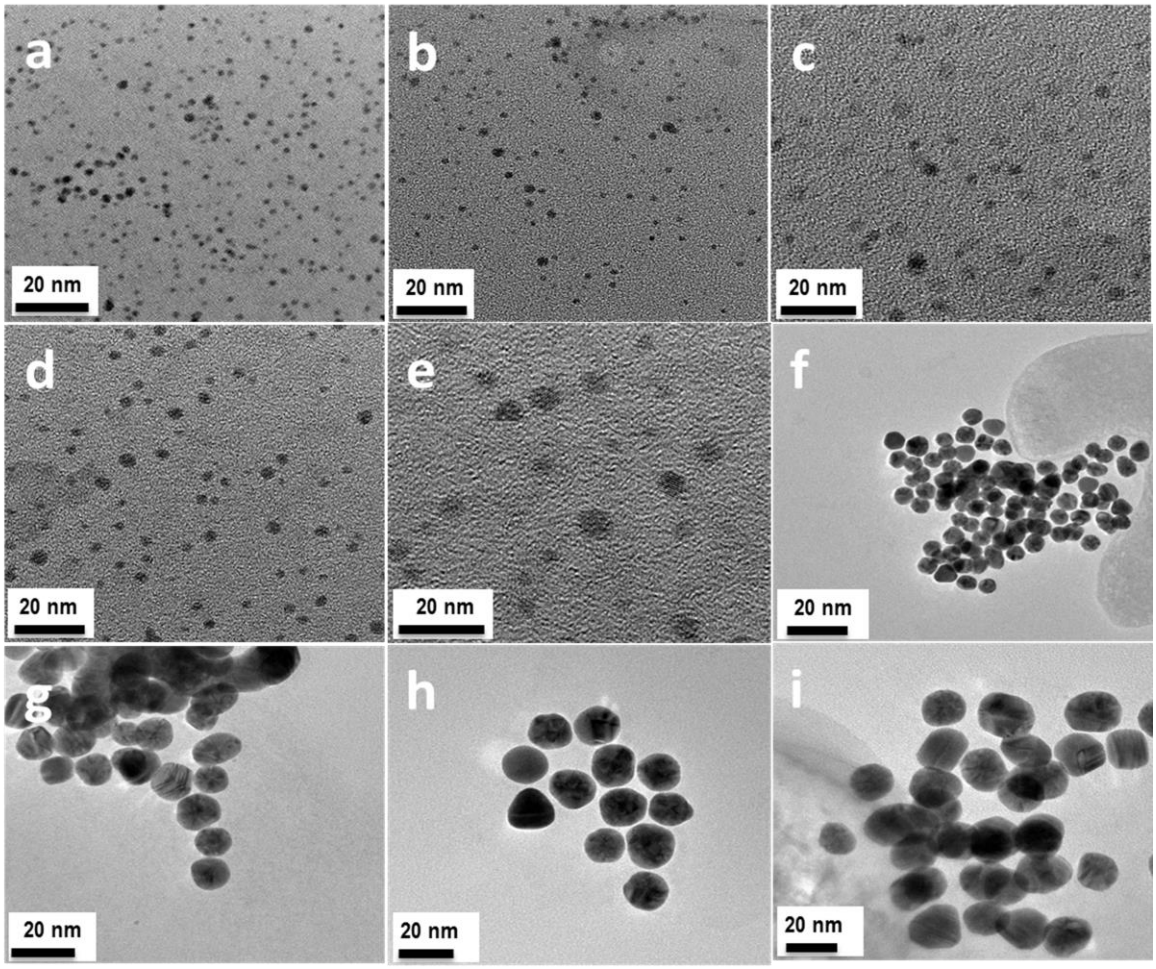

Figure 3.13. TEM images of gold nanoparticles of variable sizes of set (a) A, (b) B, (c) E, (d) F, (e) I, (f) L, (g) M, (h) N and (i) O respectively.

The theory of NSET[65] predicts surface contribution in rate of surface damping of the metal is different from the volume contribution. According to this theory, the rate of surface quenching is a function of the electron gas density parameter (r_s) while the volume damping is a function of the bulk dielectric function and therefore, the generalized rate of damping can be expressed in terms of following equation,

$$k_{ET} = \frac{1}{\tau} = \frac{\mu^2}{4d^3\hbar}F \qquad (3.8)$$

where, μ and d represents the is the dipole moment of the emitter and distance between the emitter and metal surface and F is quenching contribution from surface and volume and can be written as,

$$F_{surface} = 1.2 \frac{\omega_{dye}}{\omega_F} \frac{1}{k_F d} \quad (3.9)$$

and

$$F_{volume} = 3 \frac{\omega_{dye}}{\omega_F} \frac{1}{k_F l} \quad (3.10)$$

From these equations, we can see that, the volume quenching is a function of $1/d^3$ and the mean free path, $l(= v_F \tau')$ for the metal. Therefore, with increasing size of the particles the number density (number of particles per mL) decreasing contributes increasing mean free path because mean free path inversely proportional to the number of particles and size contribution decreases mean free path due to increasing cross-sectional area with increasing size of the particles. Therefore, a cumulative effect of size of the particles and inverse of cubic distance dependence play the key role in FRET process.

On the other hand, the surface quenching is a $1/d^4$ dependent phenomenon. The surface and the volume are indistinguishable for very small particles and hence surface quenching is observed whereas larger particles have a well-defined surface and a distinguishable volume, surface quenching is expected at shorter distances while volume quenching plays a dominant role at longer distances.[65] Therefore, calculating the surface area of the nanoparticle per milliliter of colloidal solution using the equation,

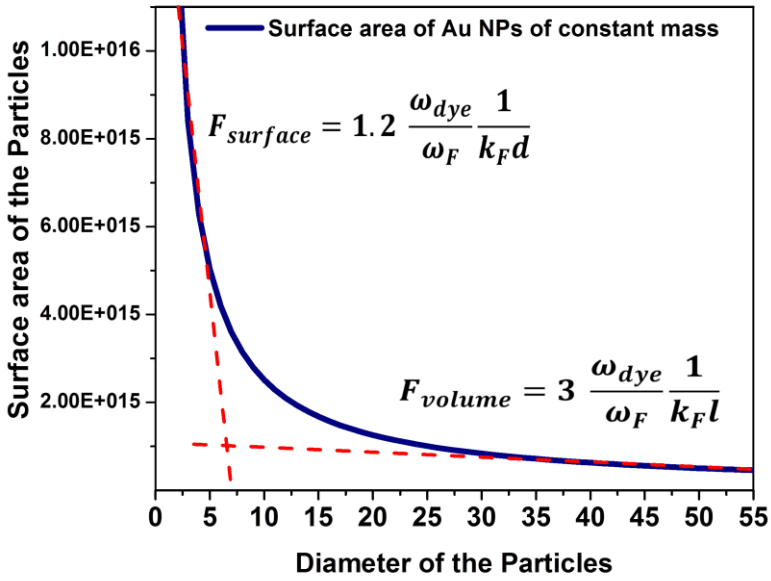

Figure 3.14. Surface area of the gold nanoparticles as a function of particle diameter at constant mass.

$$Surface\ Area = \frac{4\pi N_0 C}{1000 f}\frac{r^3}{R} \tag{3.11}$$

where, N_0 is Avogadro's Number, C is the concentration of precursor gold solution, f packing fraction of the atoms inside the particles, and r and R, the radius of atoms and particles respectively. Therefore, the plot of surface area *vs.* size of the particles at constant mass of gold is shown in Figure 3.14. distinctly shows that NSET exhibits a significant role in energy transfer process in smaller particle size regime as compared to larger particles while the FRET takes the major role in energy transfer in larger particles as compared to smaller ones. From the tangent/extrapolation of the Figure 3.14, it can easily be predicted the relying point of the NSET and FRET in between the 5 to 10 nm size regime.

FITC molecules have been used as molecular probes for the study of surface phenomena of gold nanoparticles. In this study, very dilute (0.04 μM) FITC solution has

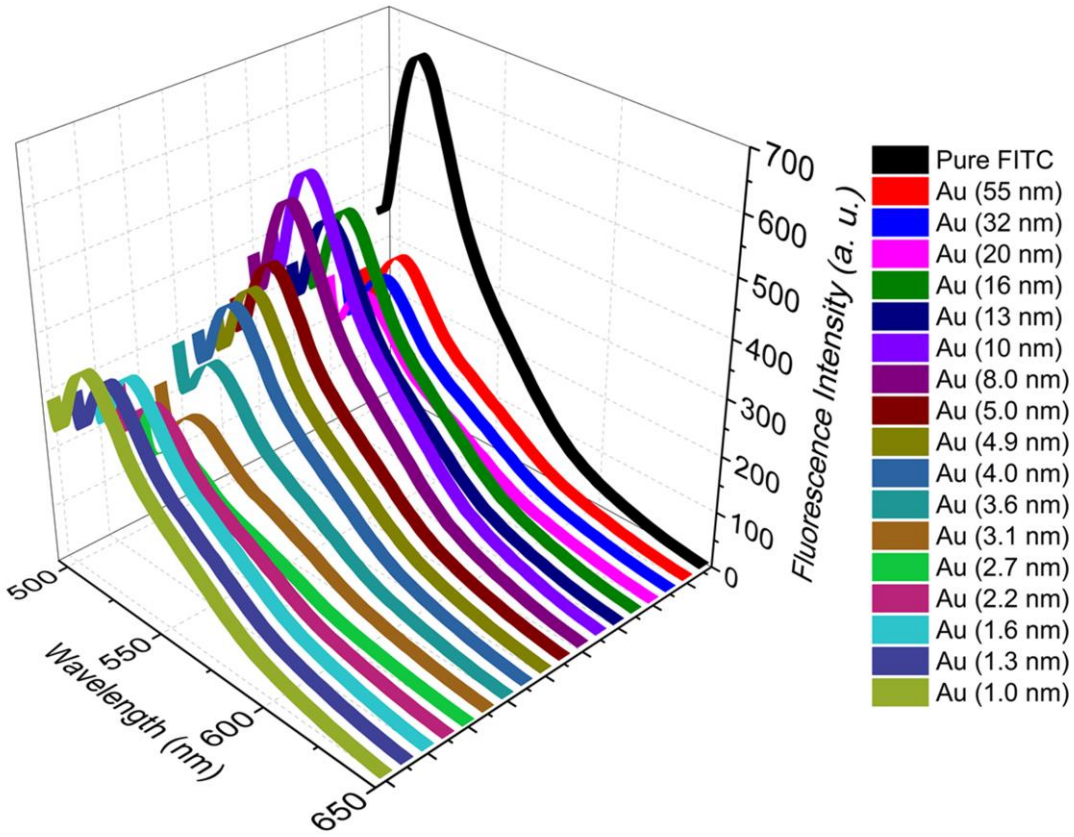

Figure 3.15. Fluorescence quenching of FITC molecules in the presence of gold nanoparticles of variable sizes.

been used to avoid the trivial effect. An aliquot of 30 μL (0.5 mM) gold nanoparticles has been added to the FITC solution and kept 2 h to attain the adsorption-desorption equilibrium between the nanoparticles and the probe molecules and the fluorescence of each solution has been measured in the spectrophotometer. From Figure 3.15, it is seen that emission from the molecular probes becomes, significantly, quenched in the presence of different sizes of gold nanoparticles. Upon careful observation, it is seen that the fluorescence quenching does not change with size of the particles in a regular manner as expected rather it exhibits some interesting results. In ultrasmall size regime of the particles, the quenching of fluorescence increases up to a particular size (2.7 nm) and then, decreases sharply for 8─10 nm gold particles. Chen et. al. have reported the dynamic quenching of fluorescence of rhodamine 6G increases upto 8-fold more efficient by varying the particle sizes from 1 to 4 nm.[75] Thereafter, fluorescence quenching, again, increases but slowly until its size is about 20 nm and then, again, quenching decreases very/negligibly slowly upto 55 nm in size. A plotting of quenching efficiency *vs.* size of the particles (Figure 3.16) that the quenching efficiency sharply increases up to 2.7 nm, then sharply decreases until 10 nm in size and then again increases but slower than earlier and finally, decreases gradually with increase in size of the particles. This phenomenon can be explained in the light of FRET and NSET mechanism.

NSET and FRET are two phenomena which strongly depend on the size of the gold nanoparticles. From Figure 3.16, we see that quenching efficiency sharply increases from 1 nm to 2.7 nm due to achieving the metallic character of the gold nanoparticles at the dimension of 2.7 nm in size.[51] Therefore, with increasing metallic character, quenching efficiency sharply increases due to NSET between the FITC and ultrasmall gold nanoparticles since small Au NPs act as point dipole. Further, with increasing size of the Au NPs particles are achieving the polarity and exhibiting the SPR on irradiation of the visible light. With increasing the size of the Au NPs, the surface properties, i. e., surface area sharply decreases and as a result, NSET sharply decreases upto 10 nm. As the size of the particles increases, the exhibited SPR become prominent with increasing absorbance, which can be represented in terms of extinction co-efficient (absorption + scattering). As a result, with increasing size of the particles, the overlap integral increases that causes increase in energy transfer and thus the quenching efficiency (10–20 nm). At the very

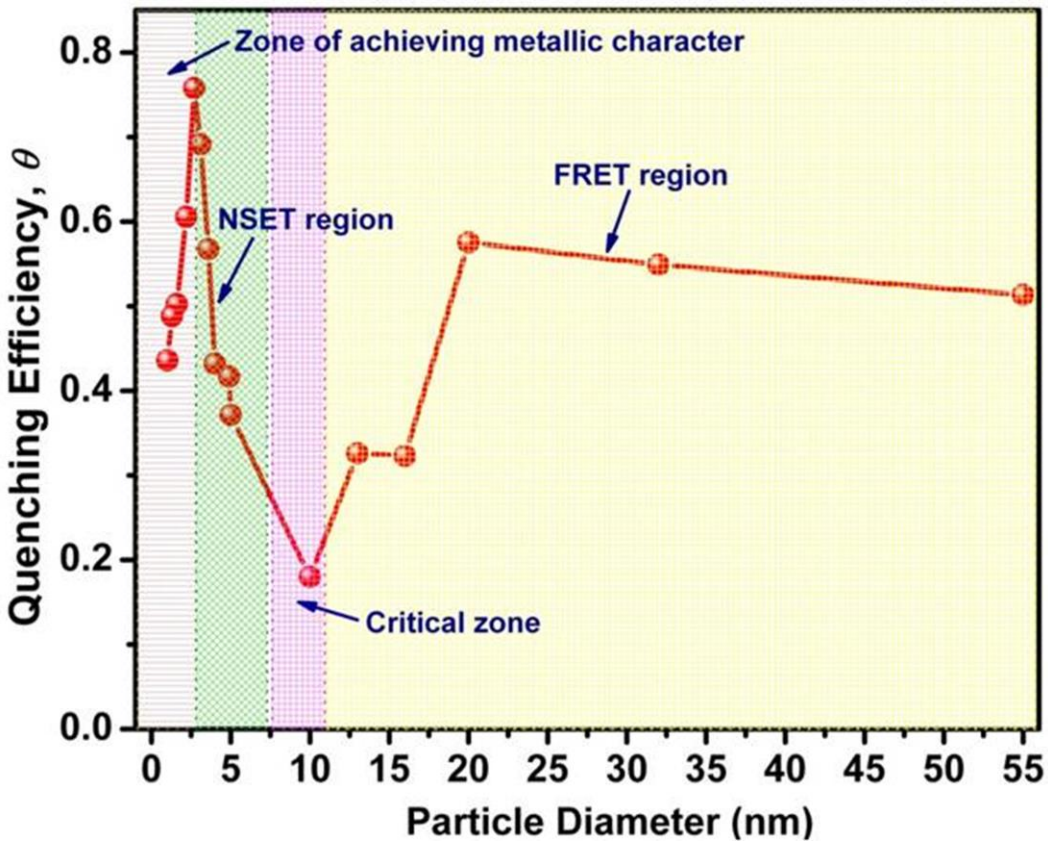

Figure 3.16. Quenching efficiency of the gold nanoparticles of FITC fluorescence as a function of particle diameter at constant mass.

high size regime of Au NPs (20−55 nm), absorption decreases though scattering increasing that decreases the overlap integral which results in slower decrease in quenching efficiency.[44]

Therefore, in Figure 3.16, 1−2.7 nm region may be coined as metallic character achieving zone. The zone of 2.7−10 nm may be represented as NSET region. Both this region is highly sensitive to the quenching efficiency of the molecular probes near the gold particles. Again, 10−55 nm region is known as FRET zone; in this zone, NSET is also possible but the probability is very less due to four reasons: (i) reducing/decreasing surface area as compared to smaller particles, (ii) decreasing interaction energy/residual force with increasing size, (iii) decreasing metal surface-FITC interaction energy due to frequent change in dipole/electronic state of the Au NPs and (iv) increase in mean free path with decreasing the number of the particles considering that other parameters, like, density, temperature to remain unaltered.

3.2.4. Conclusions

In conclusion, gold nanoparticles of variable sizes, upon interaction with fluorescein isothiocyanate, render distinct emission behavior in the two specific size regime of the particles. It is seen that quenching efficiency does not change regularly rather increases or decreases with increasing the size of the particles. Moreover, the quenching efficiency is very sensitive in smaller particle size regime. The quenching efficiency of the molecular probe in the presence of all sizes of the particles can be explained by NSET and FRET mechanism. With increasing the size of the particles, the surface area decreases and hence, NSET decreases and FRET become significant. With increasing the size of the particles, the dipole-surface interaction decreases while the dipole-dipole interaction increases. It is also observed that the quenching efficiency of the Au NPs increases with increase in the size of the particles up to a critical dimension/size and again, sharply decreases. Therefore, the present experiment offers an experimental evidence of the critical point at which the coverage of the two distance dependence process exactly occur in the particular size regime.

3.3. References

(1) Harada, Y.; Masuda, S.; Ozaki, H. *Chem. Rev.* **1997**, *97*, 1897−1952.

(2) Granqvist, C. G.; Buhrman, R. A.; Wyns, J.; Sievers, A. J. *Phys. Rev. Lett.* **1976**, *37*, 625−629.

(3) Lattuada, M.; Wu, H.; Sefcik, J. ; Morbidelli, M. *J. Phys. Chem. B* **2006**, *110*, 6574−6586 and references therein.

(4) von Smoluchowski, M. Z. *Phys. Chem.* **1917**, *92*, 129−168.

(5) Jensen, T.; Lelly, L. ; Lazarides, A. ; Schatz, G. C. *J. Cluster Sci*. **1999**, *10*, 295−317.

(6) Maria, J.; Gray, S.; Rogers, J. A.; Nuzzo, R. G. *Chem. Rev.* **2008**, *108*, 494−521.

(7) Link, S.; El-Sayed, M. A. *J. Phys. Chem. B* **1999**, *103*, 4212−4217.

(8) Mulvaney, P.; Giersig, M.; Henglein, A. *J. Phys. Chem.* **1993**, *97*, 7061−7064.

(9) Ghosh, S. K.; Pal, T. *Chem. Rev.* **2007**, *107*, 4797−4862.

(10) Liu, X.; Zhu, M.; Chen, S.; Yuan, M.; Guo, Y.; Song, Y.; Liu, H.; Li, Y. *Langmuir* **2008**, 24, 11967−11974.

(11) Liu, H.; Xu, J.; Li, Y.; Li, Y. *Acc. Chem. Res.* **2010**, 43, 1496−1508.

(12) Zheng, H.; Li, Y.; Liu, H.; Yin, X.; Li, Y. *Chem. Soc. Rev.* **2011**, *40*, 4506−4524.

(13) Kühn, S.; Hakanson, U.; Rogobete, L.; Sandoghdar, V. *Phys. Rev. Lett.* **2006**, *97*, 017402 1-3.

(14) Mühlschlegel, P.; Eisler, H. J.; Martin, O. J. F.; Hecht, B.; Pohl, D. W. *Science* **2005**, *308*, 1607−1609.

(15) Bozhevolnyi, S. I.; Volkov, V. S.; Devaux, E.; Laluet, J. Y.; Ebbesen, T. W. *Nature* **2006**, *440*, 508−511.

(16) Okamoto, K.; Niki, I.; Shvartser, A.; Narukawa, Y.; Mukai, T.; Scherer, A. *Nature Mater.* **2004**, *3*, 601−605.

(17) Atwater, H. A.; Polman, A. *Nature Mater.* **2010**, *9*, 205−213.

(18) Dulkeith, E.; Morteani, A. C.; Niedereichholz, T.; Klar, T. A.; Feldmann, J.; Levi, S. A.; van Veggel, F. C. J. M.; Reinhoudt, D. N.; Moller, M.; Gittins, D. I. *Phys. Rev. Lett.* **2002**, *89*, 203002 1−4.

(19) Mirsaleh-Kohan, N. ; Iberi, V.; Simmons, P. D. Jr.; Bigelow, N. W.; Vaschillo, A.; Rowland, M. M.; Best, M. D.; Pennycook, S. J.; Masiello, D. J.; Guiton, B. S.; Camden, J. P. *J. Phys. Chem. Lett.* **2012**, *3*, 2303−2309.

(20) Hill, R. T.; Mock, J. J.; Hucknall, A.; Wolter, S. D.; Jokerst, N. M.; Smith, D. R.; Chilkoti, A. *ACS Nano* **2012**, *6* , 9237−9246.

(21) Aslan, K.; Gryczynski, I.; Malicka, J.; Matveeva, E.; Lakowicz, J. R.; Geddes, C. D. *Curr. Opin. Biotech.* **2005**, *16*, 55−62.

(22) Zenneck, J. *Ann. Phys.* **1907**, *328*, 846−866.

(23) Sommerfeld, A. *Ann. Phys.* **1909**, *28*, 665−736.

(24) Weitz, D. A.; Garoff, S.; Gersten, J. I.; Nitzan, A. *J. Chem. Phys.* **1983**, *78*, 5324−5338.

(25) Gu, J.; Hacker, G. W. In *Gold and Silver Staining: Techniques in Molecular Morphology*, CRC, Boca Raton, Florida, 2002, pp. 107−118.

(26) Aslan, K.; Malyn, S. N.; Geddes, C. D. *J. Fluor.* **2007**, *17*, 7−13.

(27) Li, C.; Liu, X.; Yuan, M.; Li, J.; Guo, Y.; Xu, J.; Zhu, M.; Lv, J.; Liu, H.; Li, Y. *Langmuir* **2007**, *23*, 6754−6760.

(28) Lv, J.; Zhao, Y.; Li, G.; Li, Y.; Liu, H.; Li, Y.; Zhu, D.; Wang, S. *Langmuir* **2009**, *25*, 11351−11357.

(29) Kinkhabwala, A.; Yu, Z.; Fan, S.; Avlasevich, Y.; Müllen, K.; Moerner, W. E. *Nature Photonics* **2009**, *3*, 654−657.

(30) Chen, Y.; Munechika, K; Ginger, D. S. *Nano Lett*. **2007**, *7*, 690−696.

(31) Sánchez-González, Á.; Corni, S.; Mennucci, B. *J. Phys. Chem. C* **2011**, *115*, 5450−5460.

(32) Tsunoyama, H.; Sakurai, H.; Ichikuni, N.; Negishi, Y.; Tsukuda, T. *Langmuir* **2004**, *20*, 11293-11296.

(33) Imhof, A.; Megens, M.; Engelberts, J. J.; de Lang, D. T. N.; Sprik, R.; Vos, W. L. *J. Phys. Chem. B* **1999,** *103*, 1408−1415.

(34) Thorball, N. *Histochemistry* **1981**, *71*, 209−233.

(35) Linnert, T.; Mulvaney, P.; Henglein, A. *J. Phys. Chem.* **1993**, *97*, 679−682.

(36) Chandrasekharan, N.; Kamat, P. V.; Hu, J.; Jones II, G. *J. Phys. Chem. B* **2000,** *104*, 11103−11109.

(37) Mulvaney, P.; Liz-Marzan, L. M.; Giersig, M.; Ung, T.; *J. Mater. Chem.* **2000**, *10*, 1259−1270.

(38) Zhong, Z.; Patskovskyy, S.; Bouvrette, P.; Luong, J. H. T.; Gedanken, A. *J. Phys. Chem. B* **2004,** *108*, 4046−4052.

(39) Guerrero-Martínez, A.; Grzelczak, M.; Liz-Marzán, L. M. *ACS Nano* **2012**, *6*, 3655−3662.

(40) Schwartzberg, A. M.; Grant, C. D.; van Buuren, T.; Zhang, J. Z. *J. Phys. Chem. C* **2007,** *111*, 8892−8901.

(41) Albanase, A.; Chan, W. C. *ACS Nano* **2011**, *5*, 5478−5489.

(42) Zhang, Y.; Gu, C.; Schwartzberg, A. M.; Chen, S.; Zhang, J. Z. *Phys. Rev. B* **2006**, *73*, 165405−165414.

(43) Makarova, O. V.; Ostafin, A. E.; Miyoshi, H.; Norris Jr., J. R.; Meisel, D. *J. Phys. Chem. B* **1999**, *103*, 9080−9084.

(44) Ghosh, S. K.; Pal, A.; Kundu, S.; Nath, S.; Pal, T. *Chem. Phys. Lett.* **2004**, *395*, 366−372.

(45) Ghosh, S. K.; Pal, T. *Phys. Chem. Chem. Phys.* **2009**, *11*, 3831−3844.

(46) Novotny, L.; Hecht, B. In *Principles of Nano-Optics*, Cambridge University Press: New York, 2006.

(47) Bardhan, R.; Grady, N. K.; Cole, J. R.; Joshi, A.; Halas, N. J. *ACS Nano* **2009**, *3*, 744−752.

(48) Giannini, V.; Fernandez-Domínguez, A. I.; Heck, S. C.; Maier, S. A. *Chem. Rev.* **2011**, *111*, 3888−3912.

(49) Basu, S.; Panigrahi, S.; Praharaj, S.; Ghosh, S. K.; Pande, S.; Jana, S.; Pal, T. *New J. Chem.* **2006**, *30*, 1333−1339.

(50) Kim, I.; Bender, S. L.; Hrnisavljevic, J.; Utschig, L. M.; Huang, L.; Wiederrecht, G. P.; Tilde, D. M. *Nano Lett.* **2001**, *11*, 3091−3098.

(51) Varnavski, O.; Ramakrishna, G.; Kim, J.; Lee, D.; Goodson, T. *J. Am. Chem. Soc.* **2010**, *132*, 16−17.

(52) Kreibig, U.; Vollmer, M. In *Optical Properties of Metal Clusters*, Chapter 2, Springer, Berlin, 1995**,** pp. 126−128.

(53) Parker, C. A. In *Photoluminescence of Solutions*, Elsevier: Amsterdam, The Netherlands, 1981.

(54) Zuloaga, J.; Prodan, E.; Nordlander, P. *Nano Lett.* **2010**, *4*, 5269−5276.

(55) Maxwell Garnett, J. C. *Philo. Trans. R. Soc.* **1904**, *203*, 385−420.

(56) Chen, Y.; Munechika, K.; Ginger, D. S. *Nano Lett.* **2007**, *7*, 1032−1036.

(57) Carmeli, I.; Lieberman, I.; Kraversky, L.; Fan, Z. Y.; Govorov, A. O.; Markonich, G.; Richter, S. *Nano Lett.* **2010**, *10*, 2069−2074.

(58) Li, Y.; Wu, P.; Xu, H.; Zhang, H.; Zhong, X. *Analyst* **2011**, *136*, 196−200.

(59) Zhang, F.; Dressen, D. G.; Skoda, M. W. A.; Jacobs, R. M. J.; Zorn, S.; Martin, R. A.; Martin, C. M.; Clark, G. F.; Schreiber, F. *Eur. Biophys. J.* **2008**, *37*, 551−561.

(60) Vujačić, A.; Vasić, V.; Dramićanin, M.; Sovilj, S. P.; Bibić, N.; Hranisavljević, J.; Wiederrecht, G. P. *J. Phys. Chem. C* **2012**, *116*, 4655−4661.

(61) Glass, A. M.; Liao, P. F.; Bergman, J. G.; Olson, D. H. *Opt. Lett.* **1980**, *5*, 368–370.

(62) George Thomas, K.; Kamat, P. V. *J. Am. Chem. Soc.*, **2000**, *122*, 2655–2656.);

(63) Ruppin, R. *J. Chem. Phys.* **1982,** *76*, 1681-1684.

(64) Giannini, V.; Fernández-Domínguez, A. I.; Heck, S. C.; Maier, S. A.; *Chem. Rev.* **2011**, *111*, 3888–3912.

(65) Persson, B. N. J.; Lang, N. *Phys. Rev. B* **1982**, *26*, 5409–5415.

(66) Yun, C. S.; Javier, A.; Jennings, T.; Fisher, M.; Hira, S.; Peterson, S.; Hopkins, B.; Reich, N. O.; Strouse, G. F. *J. Am. Chem. Soc.* **2005**, *127*, 3115-3119.

(67) Förster, T. *Ann. Phys.* 1948, 437, 55−75.

(68) Saini, S.; Srinivas, G.; Bagchi, B. *J. Phys. Chem. B* **2009,** *113*, 1817–1832.

(69) Lakowicz, J. R. Principles of *Fluorescence Spectroscopy*, 2006, Springer Science, *LLC*.

(70) Jennings, T. L.; Singh, M. P.; Strouse, G. F. *J. Am. Chem. Soc.* **2006**, 128, 5462-5467.

(71) Tsunoyama. H.; Sakurai, H.; Tsukuda, T. *Chem. Phys. Lett.* **2006,** 429, 528–532.

(72) Frens, G. *Nature* **1973**, *241*, 20–22.

(73) Jain, P. K.; Lee, K. S.; El-Sayed, I. H.; El-Sayed, M. A. *J. Phys. Chem. B* **2006**, *110*, 7238-7248.

(74) Liu, X.; Atwater, M.; Wang, J.; Huo, Q. *Colloids and Surfaces B: Biointerfaces* **2007**, 58, 3–7.

(75) Cheng, P. P. H.; Silvester, D.; Wang, G.; Kalyuzhny, G.; Douglas, A.; Murray, R. W. *J. Phys. Chem. B* **2006**, *110*, 4637-4644.